Hindawi Publishing Corporation
International Journal of Antennas and Propagation
Volume 2013, Article ID 692915, 8 pages
http://dx.doi.org/10.1155/2013/692915

Research Article

Recovery Capabilities of Rateless Codes on Simulated Turbulent Terrestrial Free Space Optics Channel Model

A. Andò, S. Mangione, L. Curcio, S. Stivala, G. Garbo, R. Pernice, and A. C. Busacca

Department of Energy, Information Engineering and Mathematical Models (DEIM), University of Palermo, Viale delle Scienze Buiding 9, 90128 Palermo, Italy

Correspondence should be addressed to A. Andò; andrea.ando@unipa.it

Received 5 March 2013; Accepted 19 July 2013

Academic Editor: Lorenzo Luini

Free Space Optics (FSO) links are affected by several impairments: optical turbulence, scattering, absorption, and pointing. In particular, atmospheric optical turbulence generates optical power fluctuations at the receiver that can degrade communications with fading events, especially in high data rate links. Innovative solutions require an improvement of FSO link performances, together with testing models and appropriate channel codes. In this paper, we describe a high-resolution time-correlated channel model able to predict random temporal fluctuations of optical signal irradiance caused by optical turbulence. Concerning the same channel, we also report simulation results on the error mitigation performance of Luby Transform, Raptor, and RaptorQ codes.

1. Introduction

FSO is an optical wireless line-of-sight communication system able to offer good broadband performances, electromagnetic interference immunity, high security, license-free operation, low power consumption, ease of relocation, and straightforward installation [1]. It represents a modern technology significantly functional when it is impossible, expensive, or complex to use physical connections or radio links.

Thanks to these features, FSO is suitable for different broadband telecom applications as airborne, satellite scenarios, Next Generation Networks (NGN), and, finally, "Last Mile" communication links. In addition, FSO bandwidth performance can be further improved by using Wavelength Division Multiplexing (WDM) techniques reaching over 1.28 Tbps capacity [2, 3].

Unfortunately, as the transmission medium in a terrestrial FSO link is the air, these communications are strongly dependent on various atmospheric phenomena (as rain, snow, optical turbulence, and especially fog) that can cause losses and fading. Therefore, in worst-case conditions, it could be necessary to increase the optical transmission power although, at the same time, it is needed to comply with safety regulations. The commonly used wavelengths in outdoor FSO communications are 830, 1064, and 1550 nm, but, for the previously mentioned reasons, the highest is preferred for transmission [2].

Current laser technologies offer high-power sources at the most important wavelengths for communications. Novel technologies enable us to improve several applications previously limited by the fixed wavelength and power of other laser technologies. Today, we no longer have to work around the closest fit wavelength, but we can find the best wavelength to fit FSO communications [4, 5]. Moreover, new communication windows for FSO links could be explored using nonlinear optics techniques that are able to generate coherent emission at a wide range of wavelengths, from visible to THz [6–9].

The effects of already mentioned impairments are scattering (i.e., Rayleigh and Mie) losses, absorption, and scintillation. The first two can be described by proper attenuation coefficients [10] and increase if the atmospheric conditions get worse. Furthermore, hydrometeor scattering effects could introduce losses in FSO links [11], which can be estimated by proper models [12, 13]. At last, scintillation is a random phenomenon appreciable even under clear sky. It is due to atmospheric turbulences that originate local variations of the medium refractive index, thus generating optical irradiance fluctuations. Such impairments are predictable only using proper statistical models, able to describe the behavior of optical signals in free space propagation.

Therefore, due to the scintillation, in FSO links the irradiance fluctuates and could drop below a threshold under which the receiver is not able to detect the useful signal. In this case, communications suffer from cancellation errors, which cause link outages. This phenomenon becomes relevant at high distance, but it can also be observed in 500 m long FSO links. Moreover, the optical turbulence intensity can change by more than an order of magnitude during the course of a day: it reaches its maximum around midday (when the temperature is the highest) and, conversely, it is lower during the night [5].

In order to reduce or eliminate these impairments, different methods (hardware and software) were studied and reported in the literature. Hardware solutions focus on aperture averaging effects [14] to reduce irradiance fluctuations, in particular by using a bigger dimension detector or multidetector systems [15–22]. On the other hand, software techniques mostly focus on transmission codes [23–29].

Rateless codes are an innovative solution suitable for channels affected by erasure or burst errors. They add a redundant coding (also settable on the fly) to the source data, allowing the receiver to successfully recover the whole payload that, otherwise, would be corrupted or partially lost.

In order to test rateless codes recovery capabilities in FSO channels, we have to know detailed information about the occurring signal fading, in particular, its depth, temporal duration, and statistics. For this reason, we have implemented a time-correlated channel model able to generate an irradiance time series at the receiver side, at wide range of turbulence conditions (weak to strong).

Generated time series represents a prediction of temporal irradiance fluctuations caused by scintillation. By using the generated data, we were able to test the recovery capabilities of several types of rateless codes. In a previous work [23], information rates of Raptor codes and punctured LDPC codes with feedback were compared. In this paper, we instead present the FSO mitigation improvements obtained using coding schemes without any feedback.

In particular, we tested Luby Transform (LT) codes [30], Raptor codes (RCs) [31, 32], and newer RaptorQ (RQ) codes [33], for a 100 Mbps (Fast Ethernet speed) OOK modulation.

2. Channel Model

Several distribution models were developed in the literature to estimate optical turbulence effects (e.g., lognormal, negative exponential models, K-distribution) [34–38]. In detail, lognormal model is suitable for weak turbulence conditions, while negative exponential model is more appropriate for a very strong turbulence (i.e, saturate regime). Another model, which has provided excellent agreement with numerous experimental data, is the K-distribution. In particular, it is suitable under strong turbulence conditions although an extension of this model also permits us to cover weak fluctuation regimes (i.e., I-K-distribution).

Instead, a more versatile model is the Gamma-Gamma distribution, which is able to estimate optical turbulence from weak to moderate-strong fluctuation. This distribution is provided by two independent Gamma statistics which arise, respectively, from large-scale and small-scale atmospheric effects [37, 38].

For the above-mentioned properties, the Gamma-Gamma model is proper for our applications and it will be better described in Section 2.1.

2.1. Gamma-Gamma Model. The Gamma-Gamma statistics are able to describe the FSO scintillation phenomena in a broad range of turbulence conditions and, for this reason, it is suitable to design our correlated model. The Gamma-Gamma model provides the probability density function (PDF) of received optical irradiance (I) in the following form:

$$p(I) = \frac{2(\alpha\beta)^{(\alpha+\beta)/2}}{\Gamma(\alpha)\Gamma(\beta)} I^{\{[(\alpha+\beta)/2]-1\}} K_{\alpha-\beta}\left(2\sqrt{\alpha\beta I}\right), \quad (1)$$

where $\Gamma(\cdot)$ is the Gamma function and $K_n(\cdot)$ is the modified Bessel function of the second kind of order n, while α and β are two parameters expressed, for plane wave model at zero inner scale case [37], as follows:

$$\alpha = \left\{\exp\left[\frac{0.49\sigma_R^{12/5}}{\left(1+1.11\sigma_R^{12/5}\right)^{7/6}}\right]-1\right\}^{-1}$$
$$\beta = \left\{\exp\left[\frac{0.51\sigma_R^{12/5}}{\left(1+0.69\sigma_R^{12/5}\right)^{5/6}}\right]-1\right\}^{-1}, \quad (2)$$

where σ_R^2 is the Rytov variance, related to the optical turbulence: it constitutes a measure of the strength of scintillation [37, 38] and, for plane wave, is defined by

$$\sigma_R^2 = 1.23 C_n^2 k^{7/6} L^{11/6}, \quad (3)$$

where C_n^2 is the refractive index structure parameter, k is the wavenumber, and L is the path length (distance from the transmitter to the receiver).

Starting from the PDF, we can generate a random irradiance time serie, but it is mandatory to define a temporal correlation relationship between the samples. Assuming a plane-wave propagation, the spatial relationship linking the optical irradiance values is given by the following covariance function:

$$B_I(\rho) = \exp\left[\left(\frac{0.49\sigma_R^2}{\left(1+1.11\sigma_R^{12/5}\right)^{7/6}}\right) \times {}_1F_1\left(\frac{7}{6}; 1; -\frac{k(\rho)^2\eta_x}{4L}\right) + \left(\frac{0.50\sigma_R^2}{\left(1+0.69\sigma_R^{12/5}\right)^{5/6}}\right)\left(\frac{k(\rho)^2\eta_y}{L}\right)^{5/12} \times K_{5/6}\left(\sqrt{\frac{k(\rho)^2\eta_y}{L}}\right)\right] - 1, \quad (4)$$

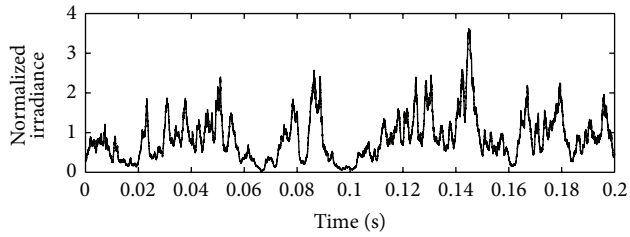

FIGURE 1: Simulated irradiance fluctuations for $\sigma_R^2 = 0.7$, at a 1550 nm wavelength, $L = 500$ m, 0.2 s time interval, and 10 μs time spacing.

where ρ is the spatial variable, ${}_1F_1(\cdot)$ is the confluent hypergeometric function of the first kind, and η_x and η_y are two parameters defined as follows [38]:

$$\eta_x = \frac{2.61}{1 + 1.11\sigma_R^{12/5}}$$
$$\eta_y = 3\left(1 + 0.69\sigma_R^{12/5}\right). \quad (5)$$

In order to convert the spatial covariance into a time function, we applied Taylor's *frozen eddies hypothesis* [37, 38]. By defining V_T as the average transverse wind speed (orthogonal to the propagation direction), we can write the following:

$$\rho = V_T t, \quad (6)$$

where t is the time.

Setting the V_T in expression (6) and substituting it into (4), the covariance becomes a function of the only independent variable t. In order to simulate our channel, we chose $V_T = 1\,\mathrm{ms}^{-1}$, thus obtaining irradiance correlation times close to those experimentally and theoretically reported in the literature [23, 39].

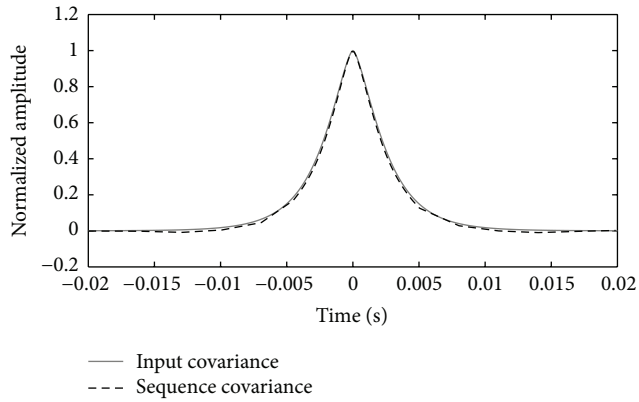

FIGURE 2: Irradiance covariance function for $\sigma_R^2 = 0.7$: input covariance and simulated irradiance sequence.

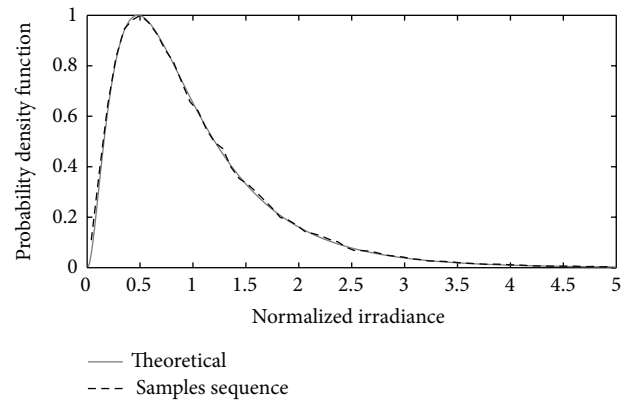

FIGURE 3: Probability density function for $\sigma_R^2 = 0.7$: theoretical and simulated irradiance samples sequence.

2.2. Non-Gaussian-Correlated Sequence. We can simulate predictions of irradiance fluctuations that make use of discrete irradiance time series—following Gamma-Gamma distribution—in which the samples are temporally spaced by one correlation time. The latter can be defined as the time in which the amplitude of normalized covariance function is equal to 0.5 and it represents a time distance beyond which we can consider the samples uncorrelated. The method that we have just described is known as Block Fading Model (BFM) [40] and it does not permit time resolution less than one correlation time. In order to reach better resolutions we have to introduce a time correlation between the irradiance samples. Unfortunately, it is not trivial to correlate a non-Gaussian distribution of samples without turning it into a Gaussian one. We can solve this problem by using a new suitable algorithm [41] defined by a correlation filter and a nonlinear memoryless block function. This algorithm is able to generate random processes with a defined marginal probability distribution and a power spectral density function (i.e., generating coloured, non-Gaussian signals). It is quite simple to be implemented as it only involves the Fourier transform and a sorting routine.

The correlation filter employed is created using the Fourier amplitudes associated with the target power spectral density. The block function is memoryless, and this ensures that the spectral properties of the generated signal are not altered during the execution of the algorithm [41].

In our case, the algorithm input parameters are the double side Fourier transform of the temporal irradiance covariance—obtained through the FFT of $B_I(t)$—and a random irradiance samples sequence that follows a Gamma-Gamma distribution. The temporal spacing between two adjacent samples is the reciprocal of the FFT sampling frequency (f_c). This means that we can choose the temporal resolution of the sequence according to our needs.

In Figure 1 we show an example of irradiance fluctuations (normalized with respect to irradiance mean value) simulation for a $\sigma_R^2 = 0.7$, at a 1550 nm wavelength, $L = 500$ m, 0.2 s time interval, and 10 μs time spacing.

Figure 2 depicts the comparison between the covariance function of the simulated irradiance fluctuations displayed in Figure 1 (dashed red line) and the input temporal covariance function (solid blue line). It is worth noting that the two above-mentioned functions are very similar: so the algorithm we used is able to properly correlate irradiance samples. We also analyze the difference between the simulated irradiance fluctuations PDF and the Gamma-Gamma distribution. Figure 3 shows that both PDFs are comparable.

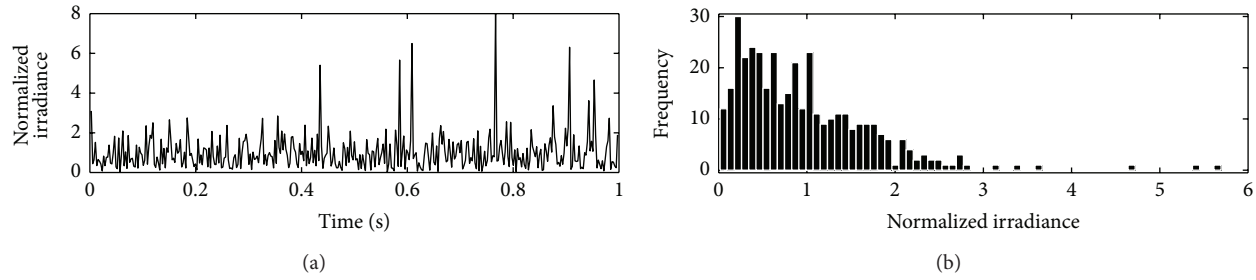

Figure 4: : (a) Samples distribution histogram and (b) simulated temporal optical irradiance fluctuations in the case of BFM.

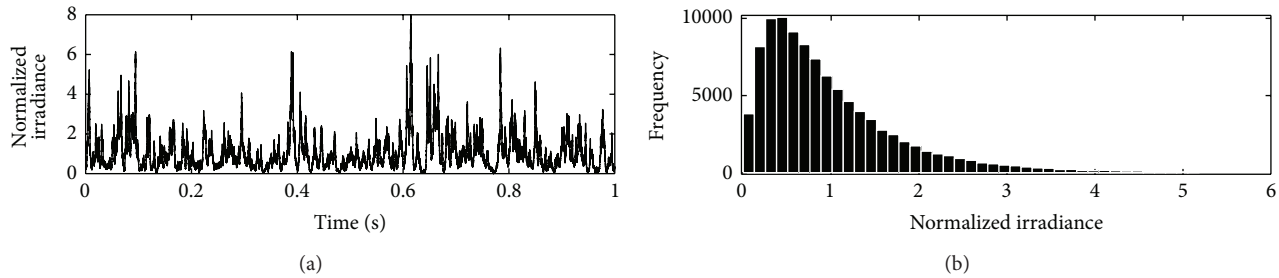

Figure 5: (a) Samples distribution histogram and (b) simulated temporal optical irradiance fluctuations in the case of correlated model.

It demonstrates that the irradiance time series exhibits the correct probability density distribution.

In the BFM the spacing between the irradiance samples equals the correlation time. We generated an irradiance time series according to the BFM, Figure 4(a), whose Gamma-Gamma distribution histogram is shown in Figure 4(b). We used $\sigma_R^2 = 1$ (value corresponding to a strong turbulence condition), a time interval of 1 s, and the correlation time value extracted from the irradiance covariance function.

In our correlated channel model, for the same values of Rytov variance and time interval, considering a temporal spacing of 10 μs, we obtained the results depicted in Figure 5. Even though the two simulations are apparently similar (as expected, since they are based on the same irradiance PDF), the correlated model has a much larger temporal resolution if compared to the BFM. For this reason, we can conclude that our model is suitable for high data rate communication tests.

3. Simulation Analysis

At the receiver, the irradiance fluctuations cause communication failures and outages, when irradiance values drop below a fading depth (threshold under which the receiver is not able to detect data). In other words, when the optical signal drops below the above-mentioned fading depth threshold, we interpret it as an erasure error occurring in the FSO communication link.

It is also worth noting that at relatively strong turbulence conditions, power fluctuations become larger and, hence, the average value of the signal power decreases. For these reasons, in our work, we referred to the normalized average value of the signal power and, in particular, to the normalized average value of the irradiance at the receiver.

Using the channel model described in the previous section, we investigated the outage statistics and the performance of rateless codes at fast data rate. In detail, we tested the LT codes and RCs capabilities in order to mitigate erasure errors, which can be detected during a 500 m single terrestrial free space link. In our simulations, we used a 1550 nm wavelength. In addition, we did not consider the noise due to the photodetector, because it can be neglected if compared to the irradiance fluctuations caused by scintillation phenomena in the turbulence conditions taken into account.

In detail, we considered that the photodetector has a Noise Equivalent Power (NEP), that is, the minimum detectable input power, of 6 dB and 9 dB lower (fading depth) than the mean value of the irradiance at the receiver. Consequently, the latter is not constant but varies with the turbulence conditions.

3.1. Outage Statistics. In Figure 6 outage statistics histograms are depicted. They correspond to a ten-hour FSO communications simulation related to two different values of σ_R^2 and to a −9 dB fading depth. We can actually see that as σ_R^2 increases, the average outage duration time grows. At different fading depths, we have found a similar behaviour. Therefore, we wondered if we were able to reduce or to eliminate communications errors by using rateless codes and, if so, what configuration parameters should be set. In order to answer these questions, we chose to employ modern code typologies belonging to rateless codes family. In particular, we used LT codes, RCs, and RQ codes.

3.2. Rateless Codes for Error Mitigation. Fountain codes (FCs) are rateless and also suitable for q-ary erasure channels; FSO channels can be described similarly. FCs do not need

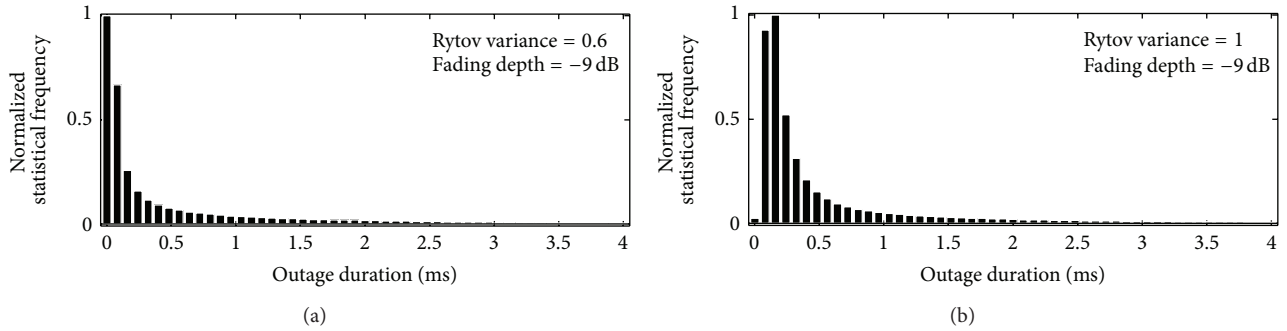

Figure 6: Outage statistics histogram for a −9 dB fading depth at a Rytov variance: (a) 0.6; (b) 1.0.

feedback [42]: in fact, they add to the source data a redundant coding (also settable on the fly) that allows the receiver to recover the whole payload, despite erasure errors. More in detail, random linear FCs for a group of K packets produce a new set of N encoded packets ($N > K$). In particular, FCs perform a linear combination (bitwise sum, modulo-2) of the K source packets by means of a binary pseudorandom **G** matrix ($K \times N$). Each generated encoded packet will be linked to one or more source packets and the number of such links is termed "degree" (δ). The **G** matrix depends on the degrees distribution and, for this reason, its definition is crucial for the code implementation. LT codes are more efficient than random linear FCs. In order to complete the decoding process, LT codes require, at least, the following two conditions: receiving a number of coded packets $O > K$ and having, for each decoding step, a coded packet with degree equal to 1. With regards to the degrees, LT codes use a robust soliton distribution [42], which guarantees, at the same overhead, a higher probability to complete the decoding process if compared to the ideal soliton distribution.

The computational costs of LT codes depend on K, but it is possible to improve their computational performance thanks to a proper management of sparse graphs. Nevertheless, the degrees distribution does not always guarantee a decoding sparse graph and, consequently, a good decoding speed. This issue is overcome with RCs. They are, substantially, LT codes in which a precoding step has been added to reduce the expected degree. In details, RCs show an expected degree equal to three. In this way, the decoding graph is always sparse and decoding computational costs are reduced.

Moreover, RCs are systematic codes (i.e., codes in which the first K encoding packets are the same as the K source packets and the last N-K repair packets are the result of encoding [43]) and they work on Galois Field 2 (GF(2)). The number of source symbols is limited to 8192 [44].

RQ codes are an evolution of RCs. They are also systematic codes but they work on a much larger alphabet, in particular on GF(256). It can be demonstrated that with a larger alphabet, the failure probability is reduced at a certain overhead [45]. Thus, RQ codes show better recovering capability. They also permit us to easily find good systematic indices [44] hence supporting a number of source symbols much larger than RCs.

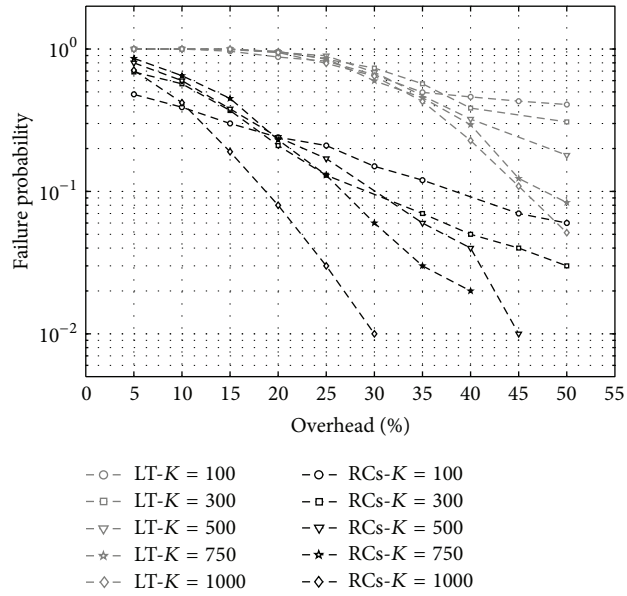

Figure 7: Comparison between LT codes and RCs for the same source packets number and overhead.

3.3. Results. We tested the performance of LT codes and RCs by simulating an OOK modulated transmission of 100 Mbps (1518 bytes frame size) over a distance of 500 m, at different fading depths and σ_R^2 values. More in detail, for each couple of the latter parameters, we evaluated the failure probabilities (for 1000 points) for an overhead ranging from 5% to 50% and for different values of K. Figure 7 shows the results concerning the case of −6 dB fading depth and $\sigma_R^2 = 1.0$. As we expected, as the overhead becomes larger, the decoding performance of both codes improves. Nevertheless, while LT codes are not always able to recover all the source data (i.e., the failure probability is always above 10^{-2}), RCs are able to recover all the source data starting from $K = 500$ and for a 50% overhead. Therefore, using the above-mentioned configurations, we were able to demonstrate that RCs failure probability can reach values below 10^{-3}.

However, the best performance is given for $K = 1000$ and starting from a 35% overhead. In Figure 8, we show the failure probability versus source packets number, for LT codes and RCs, at different overhead values. In this case, with

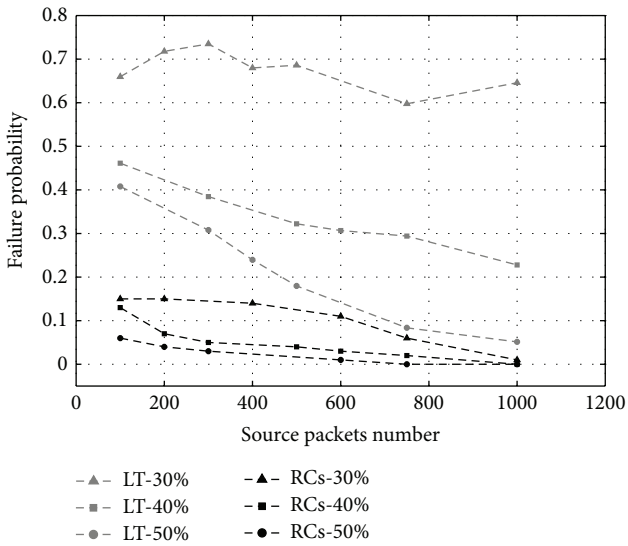

Figure 8: Comparison between LT codes and RCs at constant overhead for the same source packets number.

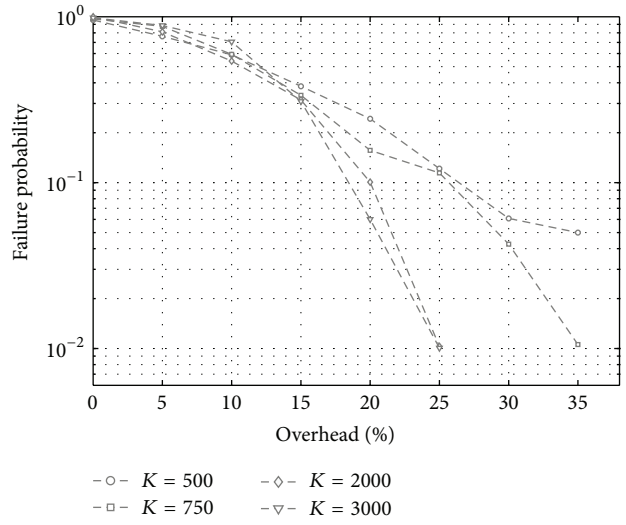

Figure 9: RQ codes at four K source packets and several overhead values.

increasing K, LT codes performance improves more than RCs one. This is due to the fact that the performance of RCs is already good even for low values of K. We carried out further tests in order to evaluate the performance of RQ codes. The same configurations we have used for LT codes and RCs have been exploited herein. The failure probability versus overhead percentage related to RQ codes is depicted in Figure 9.

We can see how RQ codes are able to recover all the source data from $K = 500$ and for a 35% overhead. For higher values of K the performance improves, so that an overhead less or equal to 25% is sufficient enough to recover data for $K > 2000$.

4. Conclusion

We produced a high-resolution FSO channel model that takes into account the temporal covariance of irradiance and hence is able to simulate the temporal irradiance fluctuations at the receiver, with a high resolution. Moreover, it also permits us to set the temporal spacing among the irradiance samples via a proper sampling frequency for the FFT of the temporal irradiance covariance. Our correlated model shows a much larger temporal resolution if compared to the BFM and, for this reason, it is appropriate for communication testing at high data rates.

We also tested, in our channel model, the performance of LT codes and RCs able to mitigate erasure errors caused by the scintillation phenomena. Our simulations illustrate that LT codes, with K values lower than 1000, are not able to cancel erasure errors, even with a 50% overhead. On the other hand, RCs can eliminate all the erasure errors, with a 50% overhead, already starting from $K = 500$. Nonetheless, RQ codes provide the best recovering performances. They work slightly better than RCs and are the best choice especially when high values of K are required.

Acknowledgments

This work is supported by the European Space Agency under Grant no. 5401001020. The authors are very grateful to Dr. E. Armandillo for enlightening discussions.

References

[1] K. Tsukamoto, A. Hashimoto, Y. Aburakawa, and M. Matsumoto, "The case for free space," *IEEE Microwave Magazine*, vol. 10, no. 5, pp. 84–92, 2009.

[2] E. Leitgeb, M. S. Awan, T. Plank et al., "Investigations on free-space optical links within SatNEx II," in *Proceedings of the 3rd European Conference on Antennas and Propagation (EuCAP '09)*, pp. 1707–1711, deu, March 2009.

[3] E. Ciaramella, Y. Arimoto, G. Contestabile et al., "1.28-Tb/s (32 × 40 Gb/s) free-space optical WDM transmission system," *IEEE Photonics Technology Letters*, vol. 21, no. 16, pp. 1121–1123, 2009.

[4] C. J. Chang-Hasnain, "Tunable vCSEL," *IEEE Journal of Selected Topics in Quantum Electronics*, vol. 6, no. 6, pp. 978–987, 2000.

[5] S. Bloom, E. Korevaar, J. Schuster, and H. Willebrand, "Understanding the performance of free-space optics," *OSA Journal of Optical Communications and Networking*, vol. 2, no. 6, pp. 178–200, 2003.

[6] A. C. Busacca, C. L. Sones, R. W. Eason, and S. Mailis, "First-order quasi-phase-matched blue light generation in surface-poled Ti:indiffused lithium niobate waveguides," *Applied Physics Letters*, vol. 84, no. 22, pp. 4430–4432, 2004.

[7] M. Cherchi, A. Taormina, A. Busacca et al., "Exploiting the optical quadratic nonlinearity of zinc-blende semiconductors for guided-wave terahertz generation: a material comparison," *IEEE Journal of Quantum Electronics*, vol. 46, no. 3, pp. 368–376, 2010.

[8] K. Kawase, T. Hatanaka, H. Takahashi, K. Nakamura, T. Taniuchi, and H. Ito, "Tunable terahertz-wave generation from DAST crystal by dual signal-wave parametric oscillation of periodically poled lithium niobate," *Optics Letters*, vol. 25, no. 23, pp. 1714–1716, 2000.

[9] A. C. Busacca, A. C. Cino, S. Riva-Sanseverino, M. Ravaro, and G. Assanto, "Silica masks for improved surface poling of lithium niobate," *Electronics Letters*, vol. 41, pp. 92–94, 2005.

[10] Recommendation ITU-R P, *Predications Method Required for Design of Terrestrial Free Space Optical Links*, 2007.

[11] R. Nebuloni and C. Capsoni, "EFfect of hydrometeor scattering on optical wave propagation through the atmosphere," in *Proceedings of the 5th European Conference on Antennas and Propagation (EUCAP '11)*, pp. 2513–2517, Rome, Italy, April 2011.

[12] M. Montopoli, F. S. Marzano, and G. Vulpiani, "Analysis and synthesis of raindrop size distribution time series from disdrometer data," *IEEE Transactions on Geoscience and Remote Sensing*, vol. 46, no. 2, pp. 466–478, 2008.

[13] S. Mori, F. S. Marzano, F. Frezza et al., "Model analysis of hydrometeor scattering effects on free space near-infrared links," in *Proceedings of the International Workshop on Optical Wireless Communications (IWOW '12)*, pp. 1–3, 2012.

[14] H. Yuksel, C. C. Davis, and L. Wasiczko, "Aperture averaging experiment for optimizing receiver design and analyzing turbulence on free space optical communication links," in *Proceedings of the Conference on Lasers and Electro-Optics (CLEO '05)*, pp. 743–745, May 2005.

[15] F. S. Vetelino, C. Young, L. Andrews, and J. Recolons, "Aperture averaging effects on the probability density of irradiance fluctuations in moderate-to-strong turbulence," *Applied Optics*, vol. 46, no. 11, pp. 2099–2108, 2007.

[16] M.-A. Khalighi, N. Schwartz, N. Aitamer, and S. Bourennane, "Fading reduction by aperture averaging and spatial diversity in optical wireless systems," *Journal of Optical Communications and Networking*, vol. 1, no. 6, Article ID 5338662, pp. 580–593, 2009.

[17] A. Hashmi, A. Eftekhar, S. Yegnanarayanan, and A. Adibi, "Analysis of optimal adaptive optics system for hybrid rf-wireless optical communication for maximum efficiency and reliability," in *Proceedings of the 4th IEEE International Conference on Emerging Technologies (ICET '08)*, pp. 62–67, October 2008.

[18] S. M. Navidpour, M. Uysal, and M. Kavehrad, "BER performance of free-space optical transmission with spatial diversity," *IEEE Transactions on Wireless Communications*, vol. 6, no. 8, pp. 2813–2819, 2007.

[19] T. A. Tsiftsis, H. G. Sandalidis, G. K. Karagiannidis, and M. Uysal, "Optical wireless links with spatial diversity over strong atmospheric turbulence channels," *IEEE Transactions on Wireless Communications*, vol. 8, no. 2, pp. 951–957, 2009.

[20] E. Bayaki, R. Schober, and R. K. Mallik, "Performance analysis of MIMO free-space optical systems in Gamma-Gamma fading," *IEEE Transactions on Communications*, vol. 57, no. 11, pp. 3415–3424, 2009.

[21] A. García-Zambrana, C. Castillo-Vázquez, and B. Castillo-Vázquez, "Outage performance of MIMO FSO links over strong turbulence and misalignment fading channels," *Optics Express*, vol. 19, no. 14, pp. 13480–13496, 2011.

[22] Z. Hajjarian, J. Fadlullah, and M. Kavehrad, "MIMO free space optical communications in turbid and turbulent atmosphere," *Journal of Communications*, vol. 4, no. 8, pp. 524–532, 2009.

[23] J. A. Anguita, M. A. Neifeld, B. Hildner, and B. Vasic, "Rateless coding on experimental temporally correlated fso channels," *Journal of Lightwave Technology*, vol. 28, no. 7, pp. 990–1002, 2010.

[24] I. B. Djordjevic, B. Vasic, and M. A. Neifeld, "Multilevel coding in free-space optical MIMO transmission with Q-ary PPM over the atmospheric turbulence channel," *IEEE Photonics Technology Letters*, vol. 18, no. 14, pp. 1491–1493, 2006.

[25] F. Xu, M. A. Khalighi, and S. Bourennane, "Pulse position modulation for FSO systems: Capacity and channel coding," in *Proceedings of the 10th International Conference on Telecommunications (ConTEL '09)*, pp. 31–38, June 2009.

[26] A. Andò, S. Mangione, L. Curcio et al., "Rateless codes performance tests on terrestrial FSO time-correlated channel model," *Proceeding of the IEEE of the International Workshop on Optical Wireless (IWOW '12)*, 2012.

[27] I. B. Djordjevic, "LDPC-coded MIMO optical communication over the atmospheric turbulence channel using Q-ary pulse-position modulation," *Optics Express*, vol. 15, no. 16, pp. 10026–10032, 2007.

[28] K. Fatima, S. S. Muhammad, and E. Leitgeb, "Adaptive coded modulation for FSO links," in *Proceeding of IEEE the International Syposium on Communication Systems, Networks & Digital Signal Processing (CSNDSP '12)*, pp. 1–4, 2012.

[29] N. Kumar, V. K. Jain, and S. Kar, "Evaluation of the performance of FSO system using OOK and M-PPM modulation schemes in inter-satellite links with turbo codes," in *Proceedings of the 1st International Conference on Electronics Communication and Computing Technologies (ICECCT '11)*, pp. 59–63, ind, September 2011.

[30] M. Luby, "LT codes," in *Proceedings of the 34rd Annual IEEE Symposium on Foundations of Computer Science*, pp. 271–280, can, November 2002.

[31] A. Shokrollahi, "Raptor codes," *IEEE Transactions on Information Theory*, vol. 52, no. 6, pp. 2551–2567, 2006.

[32] M. Luby, A. Shokrollahi, M. Watson, and T. Stockhammer, *Raptor Forward Error Correction Scheme for Object Delivery*, RFC, 5053—Proposed Standard, IETF, 2007.

[33] M. Luby, A. Shokrollahi, M. Watson, T. Stockhammer, and L. Minder, *RaptorQ Forward Error Correction Scheme for Object Delivery*, RFC, 6330—Proposed Standard, IETF,, 2007.

[34] S. Karp, R. M. Gagliardi, S. E. Moran, and L. B. Stotts, *Optical Channels: Fibers, Clouds, Water and the Atmosphere*, Plenum Press, New York, NY, USA, 1988.

[35] G. R. Osche, *Optical Detection Theory for Laser Applications*, Wiley, New Jersey, NJ, USA, 2002.

[36] J. W. Goodman, *Statistical Optics*, Wiley, New York, NY, USA, 1985.

[37] L. C. Andrews, R. L. Phillips, and C. Y. Hopen, *Laser Beam Propagation Through Random Media*, SPIE Press, Bellingham, Wash, USA, 2nd edition, 2005.

[38] L. C. Andrews, R. L. Phillips, and C. Y. Hopen, *Laser Beam Scintillation With Applications*, SPIE Press, Bellingham, Wash, USA, 2001.

[39] F. Dios, J. Recolons, A. Rodríguez, and O. Batet, "Temporal analysis of laser beam propagation in the atmosphere using computer-generated long phase screens," *Optics Express*, vol. 16, no. 3, pp. 2206–2220, 2008.

[40] F. Xu, A. Khalighi, P. Caussé, and S. Bourennane, "Channel coding and time-diversity for optical wireless links," *Optics Express*, vol. 17, no. 2, pp. 872–887, 2009.

[41] J. M. Nichols, C. C. Olson, J. V. Michalowicz, and F. Bucholtz, "A simple algorithm for generating spectrally colored, non-Gaussian signals," *Probabilistic Engineering Mechanics*, vol. 25, no. 3, pp. 315–322, 2010.

[42] D. J. C. MacKay, "Fountain codes," *IEE ProceedIngs*, vol. 152, no. 6, pp. 1062–1068, 2005.

[43] J. Lacan, V. Roca, J. Peltotalo, and S. Peltotalo, *Reed-Solomon Forward Error Correction (FEC) Schemes*, RFC, 5510—Standard Tracks, IETF, 2009.

[44] A. Shokrollahi and M. Luby, "Raptor codes," *Foundations and Trends in Communications and Information Theory*, vol. 6, no. 3-4, pp. 213–322, 2009.

[45] C. Bouras, N. Kanakis, V. Kokkinos, and A. Papazois, "Enhancing reliable mobile multicasting with RaptorQ FEC," in *Proceedings of the IEEE Symposium on Computers and Communications (ISCC '12)*, pp. 000082–000087, 2012.